



# Effect of illumination and applied potential on the electrochemical impedance spectra in triple cation (FA/MA/Cs) 3D and 2D/3D perovskite solar cells

Sumayya M. Abdulrahim<sup>a</sup>, Zubair Ahmad<sup>a,b,\*</sup>, Muhammad Qasim Mehmood<sup>c</sup>, Sanghyun Paek<sup>d</sup>, J. Bhadra<sup>a</sup>, Noora J. Al-Thani<sup>a</sup>, Mohammad Khaja Nazeeruddin<sup>e</sup>, Abdelhak Belaidi<sup>f</sup>, Mahmood Amani<sup>f</sup>

<sup>a</sup> Qatar University Young Scientists Center (QUYSC), Qatar University, Doha 2713, Qatar

<sup>b</sup> Center for Advanced Materials (CAM), Qatar University, Doha 2713, Qatar

<sup>c</sup> NanoTech Lab, Department of Electrical Engineering, Information Technology University (ITU) of the Punjab, Ferozepur Road, Lahore 54600, Pakistan

<sup>d</sup> Department of Chemistry and Energy Engineering, Sangmyung University, Seoul 03016, Republic of Korea

<sup>e</sup> Group for Molecular Engineering of Functional Materials, Institute of Chemical Sciences and Engineering, EPFL VALAIS, Sion 1951, Switzerland

<sup>f</sup> Petroleum Engineering, Texas A&M University at Qatar, Education City, PO Box 23874, Doha, Qatar

## ARTICLE INFO

### Keywords:

3D & 2D/3D perovskite solar cells  
Electrochemical impedance spectroscopy  
Degradation  
Aging

## ABSTRACT

Even though there has been numerous works performed based on electrochemical impedance spectroscopy (EIS) of perovskite solar cells (PSCs), however, many aspects of the obtained EI spectra are yet to be fully grasped. Moreover, the change of these spectra over the passage of time needs to be fully analysed and understood, therefore, this research aimed to perform a comparative study to provide a comprehensive understanding of the illumination and voltage dependence of impedance spectra of 3D & 2D/3D PSCs with aging time. The analysis was performed over the period of 5000 h of exposure of the PSCs to the ambient environment at room temperature ( $24 \pm 1$  °C). Complex EIS curves (nyquist plots and bode plots) have been investigated (with aging) in the dark, under 1 Sun illumination and at different applied potentials. Over the course of time, the charge transfer resistance ( $R_{ct}$ ) trend of both solar cells types was observed to be behaving oppositely in the dark and under illumination in the short circuit condition. Moreover, at high potentials in dark conditions, a negative capacitance feature was observed, while under 1 Sun illumination, this feature was realized even at low potentials. All of these complex observations have been interpreted and explained in terms of the charge dynamic in bulk and at the interfaces of 3D and 2D/3D PSCs. This study paves the way to understand further the complex charge dynamic processes within PSCs that evolve under different operating conditions with aging.

## 1. Introduction

The lab-scale efficiency of organic-inorganic halide-based perovskite solar cells (PSCs) has already reached above 25% [1,2] which is on par with the commercial silicon solar cells. However, the lack of durability of PSCs has restricted them from penetrating into the commercial market. Despite the fact that a remarkable stability has been obtained by employing a 2D capping layer over 3D perovskite layer [3–7], still a further work is necessary to establish a complete understanding underlying device physics and interface chemistry of these devices. Several techniques have been used in previous works for a comparative analysis of 3D and 2D/3D PSCs, including SEM, STEM,

XRD, electric field induced second harmonic generation (EFISHG) and electrochemical impedance spectroscopy (EIS). For instance, Cho *et al.* [8], has compared the 2D/3D PSC structure with the 3D PSC by SEM, J-V characterization and EIS techniques. They showed that the 2D perovskite (over the 3D) coating led to a smoother morphology as compared to the 3D PSC structure. In the nyquist plot, the low frequency arcs were analyzed and it was observed that the arc of 2D/3D PSC was two times bigger indicating that the recombination resistance increased twice from 3D to 2D/3D PSC. Ahmad *et al.* [4] also compared the stability of 3D PSCs with 2D/3D PSCs by EFISHG and EIS techniques under light and heat soaking to understand the charge carrier behavior. The results showed that the EFSIHG intensity reduced

\* Corresponding author at: Qatar University Young Scientists Center (QUYSC), Qatar University, Doha 2713, Qatar.  
E-mail address: [zubairtarar@qu.edu.qa](mailto:zubairtarar@qu.edu.qa) (Z. Ahmad).

significantly in 3D as compared to 2D/3D PSC samples. EFSIHG intensity is directly related to induced polarization in PSCs. The higher the polarization under a specific applied voltage, the higher the EFSIHG intensity. A decrease in EFSIHG intensity with time can be directly linked to the degradation of PSC samples. EIS analysis of the same samples were also performed and the resultant spectra depicted that comparatively less resistance was provided to the flowing electrons in the 2D/3D PSC samples. On the other hand, some studies on 3D and 2D/3D perovskites are limited to just a general characterization of solar cells that includes J-V curves, SEM, STEM, XPS, GDOES and XRD patterns to study the optical and structural properties of the PSCs [6,9–11]. J-V characteristic curves help us determine the performance of the PSCs in terms of their power conversion efficiencies, whereas the SEM images and XRD patterns give us an insight into the thickness and morphology of the layers in a PSC. To analyze each layer of the PSC, SEM is usually used after the fabrication of every layer. Moreover, to analyze the internal structural properties of the PSCs, a cross-sectional STEM is required and hence can be considered as a destructive technique [8]. Besides, these techniques lack a deep understanding of the interfacial mechanisms at the 2D/3D heterojunction and the relative contributions of the mobile ionic and trapped charge carriers. Therefore, in this respect, EIS technique is an appealing and frequently employed tool used for studying the simultaneously occurring dynamic processes in the multiple layered-nanostructured PSCs. EIS utilizes a frequency-domain technique where the various dynamic processes can be distinguished and hence each process can be analyzed individually. However, the existing EIS analysis of the PSCs reported in the recently published work still needs to further extend to get a deeper insight.

Firstly, the effect of light radiation on EIS is irrespective of applied potential [12]. Therefore, it is essential to treat light and voltage as independent parameters. For instance, Bernal *et al.* [13], discusses the complications related to analyzing the EIS due to ion dynamics and seeks to provide a more in-depth characterization by analyzing the PSCs with different experimental variables such as temperature and illumination. The data in this study is then analyzed by quantifying recombination losses and charge collection. Light radiation is one of the essential requirements for ion kinetics and incrementing ion conductivity [14]. Similarly, the voltage also has a strong influence on EIS since the PSCs respond differently under different biasing conditions. Liu *et al.* [15] utilized EIS tool to study the trend of charge transfer resistance of 3D and 2D/3D PSC against a range of applied potential (0 V – 1.1 V) and found out that the charge transfer resistance decreases substantially in the high biasing region which was attributed to improved charge transfer across the perovskite/HTM interface in 2D/3D PSC.

Secondly, the aging factor is either completely ignored in many EIS studies or has been investigated over a shorter period of time. For example, Choi *et al.* [5] performed a comparative study of 3D of

2D/3D PSC over a period of 1000 h. The charge recombination trend was studied using EIS tool and it was found that the addition of 2D capping layer results in an enhanced charge recombination resistance. Mahapatra *et al.* [16] utilized EIS tool to study the aging process of PSCs, over a period of 96 h and concluded that the low-frequency capacitance increases with aging due to charge accumulation. Klotz *et al.* [17] also shines a light on the importance of unsteady EIS study to help quantify ion dynamics. High-frequency semicircles of the nyquist plots are studied in his paper to understand charge dynamics.

Overall, only a limited comparative studies of 3D and 2D/3D PSCs have been performed, utilizing EIS tool to study the effect of illumination, voltage and aging together. Therefore, further studies on this topic, utilizing EIS tool are crucial to elucidate further comprehensive depictions of the aging process of 3D and 2D/3D PSC under light and different applied potentials over the longer period. We have previously performed various aging studies on 3D and 2D/3D PSCs where the effects of degradation on stability were realized using EIS technique [18–20]. Recently our group performed a study specifically focusing on the charge transfer, Au/HTM/perovskite interface over a period of 6 months [18]. Next, we performed a longer study of upto 24 months using EIS to analyze the charge transfer and recombination in 3D and 2D/3D PSCs [20]. However, in our previous works, the analysis was performed only at 0 V under dark conditions. Moving forward, we believe that an aging study under different applied potentials and illumination is crucial to obtain a more practical understanding of the evolution of charge dynamics of 3D and 2D/3D PSCs. Therefore, the current study aims to analyze the complete EI spectra under illumination and in dark conditions at 0 V, 0.5 V and 1.1 V, with aging (5000 h). To physically interpret the system, an equivalent circuit model was developed, which comprises of resistance elements as well as the capacitance and inductance elements [21]. This analysis was performed to quantitatively assess the series, charge transfer and charge recombination resistances under different operating conditions with the objective of a comprehensive analysis of the PSCs behavior.

## 2. Experimental procedure

### 2.1. Device fabrication

The 3D and 2D/3D PSCs were fabricated as reported previously [18]. In brief, 3D and 2D/3D PSCs were fabricated based on *n-i-p* architecture. The ETL layer (compact TiO<sub>2</sub>, c-TiO<sub>2</sub>) was deposited on FTO coated glass by spray pyrolysis at 450 °C. Subsequently, mesoporous TiO<sub>2</sub> (m-TiO<sub>2</sub>) layer was deposited by spin coating at 5000 rpm for 20 s followed by 30 min of annealing at 500 °C. Next, a tin oxide passivation layer was spin-coated on the substrate at 3000 rpm for 30 secs at 100 °C, followed by 60 min of annealing at 190 °C. Next, 37  $\mu$ l of triple cation (FA/MA/Cs) 3D-perovskite precur-

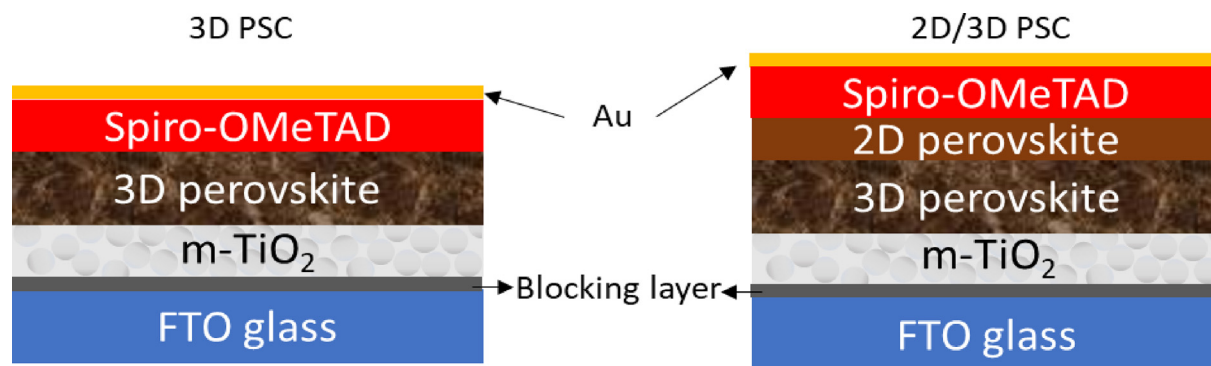


Fig. 1. Illustrative representation of 3D and 2D/3D PSC fabricated for this work. The additional 2D layer in 2D/3D PSCs protects the 3D layer from outer environment.

sor was deposited on the substrate in a glove box with nitrogen environment (20 to 25% RH) by a two-step spin coating at 2000 rpm for 12 secs and 5500 rpm for 30 secs. The final perovskite prepared was  $\text{Cs}_{0.1}\text{-FA}_{0.76}\text{MA}_{0.14}\text{PbI}_{2.58}\text{Br}_{0.42}$ . 110  $\mu\text{l}$  of chlorobenzene was deposited on the spinning substrate after 25% completion of the previous step. The sample was then annealed for 60 min at 100 °C to obtain 3D-perovskite crystals. To obtain the 2D perovskite layer, the precursor (PEAI dissolved in isopropanol), was spin-coated at 4200 rpm for 20 secs, on top of the 3D layer. Next, 37  $\mu\text{l}$  of the SpiroOMeTAD precursor salt was spin-coated on the substrate. The spiro was doped with cobalt salt ( $\text{Co}[\text{t-BuPyPz}]_3[\text{TFSI}]_3$ ) and lithium salt (Li-TFSI). 4-tertbutylpyridine (TBP) was also added. Finally, a 70 nm thick gold layer was thermally deposited on both samples. Fig. 1 represent the schematic diagram of 3D and 2D/3D PSCs fabricated for this work.

## 2.2. Device characterization

The evolution in  $J_{\text{sc}}$ ,  $V_{\text{oc}}$ , FF, and PCE of the prepared 3D and 2D/3D devices were measured by conducting I-V characterization on fresh samples, after 2500 h and after 5000 h of exposure to ambient environment at room temperature ( $24 \pm 1$  °C). The characterization was performed by keeping the samples in Abet Technology SunLite Solar Simulator and measuring the current against an externally applied biasing using a digital Source Measurement Unit (Keithley 2400). Next, electrochemical impedance spectroscopy (EIS) analysis was performed in the dark and 1 sun illumination conditions at 0 V, 0.5 V, and 1.1 V biasing using Gamry 3000 potentiostat, in the frequency range of 1 MHz – 0.1 mHz. Firstly, the study was performed in the dark at a fixed biasing, with aging, to analyze the evolution of charge dynamics with time (EIS measurements were performed in two cycles; after 1000 h and 5000 h of fabrication). The first EIS measurement was taken after 1000 h and not on fresh samples because the EIS results tend to be unstable when freshly fabricated as reported previously [20]. Therefore, the samples were left to age for 1000 h before taking the first EIS measurement. Next, the analysis was performed at a fixed aging time with different biasing conditions (0 V, 0.5 V, 1.1 V) to study the impact of voltage. Finally, the study was performed under 1 Sun illumination to understand its effect on the impedance response of 3D and 2D/3D PSCs. The EIS measurements under light were performed in three cycles; after 1000 h, 2500 h and 5000 h of fabrication. The additional EIS measurement under light (2500 h) was taken to better explain the complex evolution of EIS curves under illumination, with aging. The 3D and 2D/3D samples were masked to define an active area of 0.16  $\text{cm}^2$ . An AC perturbation of 10 mV was applied under dark and light conditions, to allow charge movement. Finally, to interpret the EIS results, electrical equivalent circuit (EEC) modelling was performed to fit the data, using Gamry Echem Analyst software. XRD and SEM have been performed to study morphology and verify the presence of the 2D layer.

## 3. Results and discussion

Fig. 2a shows the XRD patterns of 3D, 2D ( $\text{PEA}_2\text{PbI}_4$ ) and 2D/3D films (on  $\text{TiO}_2/\text{FTO}$  substrates). The 2D/3D perovskite films showed extra peaks at 5.44°, 10.81°, 16.31°, 21.71° and 27.31° compared to 3D film. Specifically, the newly formed peak at 5.44° makes it very obvious that an additional film is present other than the 3D film. The main 3D film peak at 14.1° was also observed in the 2D/3D film without shifting or disappearing confirming that a separate layer (2D) had been formed over the 3D layer. Moreover, the peak positions of 2D/3D and 2D perovskite layer were found to be consistent indicating that it indeed is the 2D layer formed over the 3D (the presence of 2D layer was confirmed). Fig. 2b shows the top view SEM images of 3D and 2D/3D perovskite films. It is clear from the SEM images that the 3D perovskite film has clear grains with sharp edges as well as small

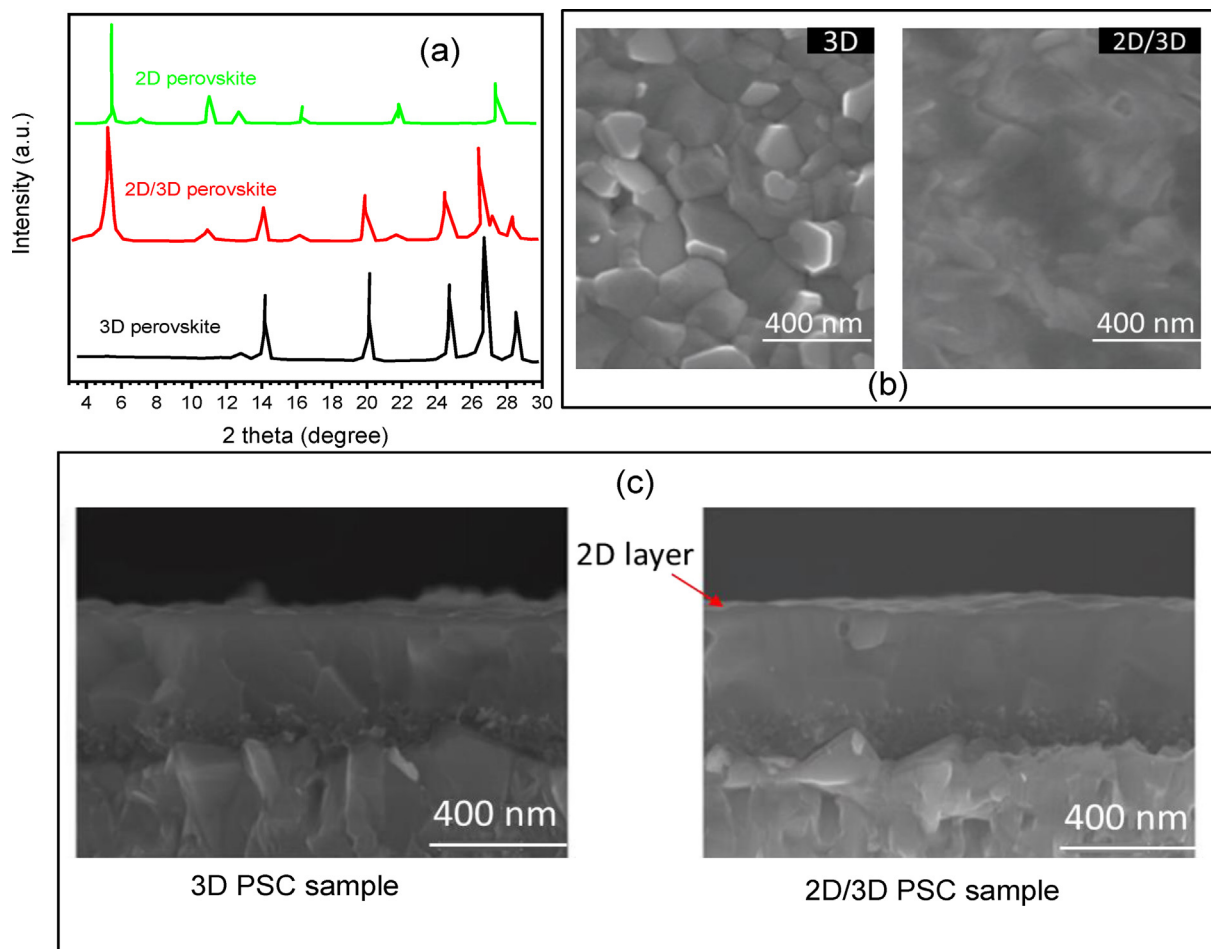
voids between the grains. On the other hand, the 2D perovskite film looks like a gel spread on top of the 3D film which provides a more uniform coating over the 3D film. The same observation can be made from the cross-sectional SEM (Fig. 2c) of 3D and 2D/3D samples where the surface morphology can be visualized to be more homogenous in the 2D/3D sample compared to that of the 3D sample.

Fig. 3(a and b) shows the J-V characterization of the 3D and 2D/3D samples, respectively. The J-V characteristics were recorded over the different intervals of time including, fresh samples (first cycle), after 2500 h (second cycle), and after 5000 h (third cycle) of fabrication. Graphs given in the insets of Fig. 3 show the change in the photovoltaic parameters of both the solar cell types with aging. As it can be observed, the change in photovoltaic parameters in 3D PSC was more drastic compared to 2D/3D PSC. In the case of 3D sample, the PCE decreased from 19.01% to 5.16% and 2.70% after 2500 h and 5000 h of ambient exposure, respectively, as shown in Table 1. The  $J_{\text{sc}}$  dropped from 23.18 to 4.99  $\text{mA}/\text{cm}^2$ ,  $V_{\text{oc}}$  decreased from 1.07 V to 1.025 V and FF changed from 78.3% to 53.4 % within 5000 h. On the other hand, the J-V characterization analysis of 2D/3D sample showed a PCE decrease from 19.8% to 12.04%, after 2500 h and further to 8.60% after 5000 h of aging in ambient conditions. The values of  $J_{\text{sc}}$  and FF dropped from 23.29  $\text{mA}/\text{cm}^2$  and 79.2 to 14.1  $\text{mA}/\text{cm}^2$  and 56.4, respectively. However no noticeable decrease was seen in  $V_{\text{oc}}$  for the case of 2D/3D device. Moreover, the decrease in PCE of 2D/3D sample was also less pronounced to that of the 3D sample, as expected. This could be because the 2D protection layer over the 3D perovskite, prevents moisture penetration to the device which enhances the stability of the device.

The J-V characteristic plots helped us quantify the photovoltaic parameters with the passage of time. However, to get a detailed insight into the evolution of interfacial dynamic processes with time, electrochemical impedance spectroscopy (EIS) analysis, was performed. 3D and 2D/3D PSC samples were analyzed in the dark, under 1 sun illumination, and under different applied potentials (0 V, 0.5 V and 1.1 V). The evaluation of the data using EEC analysis can provide us with information about charge dynamic processes at the interfaces.

There are several parameters, which are responsible for charge dynamics in the PSCs, that can be extracted from the EI spectra. These parameters include the series resistances ( $R_s$ ), high-frequency (HF) resistance linked to charge transfer ( $R_{\text{ct}}$ ) [18]. The intermediate to low frequency (IF – LF) region is related to recombination and ionic diffusion processes and their associated capacitive components [20]. These parameters can be quantitatively assessed by an electrical equivalent circuit (EEC) modeling. The 3D and 2D/3D PSC devices were fitted according to the EEC model shown in Fig. 4. Table 2 has been developed showing the EEC models used for 3D and 2D/3D samples fitting under each specified conditions (applied potential and dark or light measurements). The contribution from the 2D layer in 2D/3D device can be represented by an additional RC element in EEC modelling. However, our EEC results did not show an additional distinguished time constant in 2D/3D sample. Therefore, both 3D and 2D/3D samples were fitted following the same EEC current flow model. Nevertheless, the EEC fitted EIS parameters of the 2D/3D sample were significantly different from that of the 3D sample implying the contribution from 2D layer.

As it can be observed in Table 2, at low and high potentials, 3 RC model can be used to fit the EI spectra. At low potentials the m- $\text{TiO}_2$  layer provides a very high resistive path for the current flow as compared to the c- $\text{TiO}_2$ /perovskite interface, therefore does not contribute to the current flow model. In contrast, at high potentials, the c- $\text{TiO}_2$ /perovskite interface contribution can be ignored due to the relatively high resistance (compared to m- $\text{TiO}_2$  layer) and minimum capacitance [22] as demonstrated in the conditions mentioned in the Fig. 4 (zoom in section). However, at intermediate potentials, an additional RC element needs to be added due to the multiple contributions, from both c-



**Fig. 2.** (a) XRD patterns of 3D perovskite film ( $\text{Cs}_{0.1}\text{FA}_{0.74}\text{MA}_{0.13}\text{PbI}_{2.48}\text{Br}_{0.39}$ ), 2D/3D perovskite film layered 3D and 2D perovskite film ( $\text{PEA}_2\text{PbI}_4$ ), performed in grazing incident mode. (b) SEM image (top view) of 3D perovskite film (left) and 2D/3D perovskite film (right). (c) cross-sectional SEM of 3D PSC (left) and 2D/3D PSC (right).

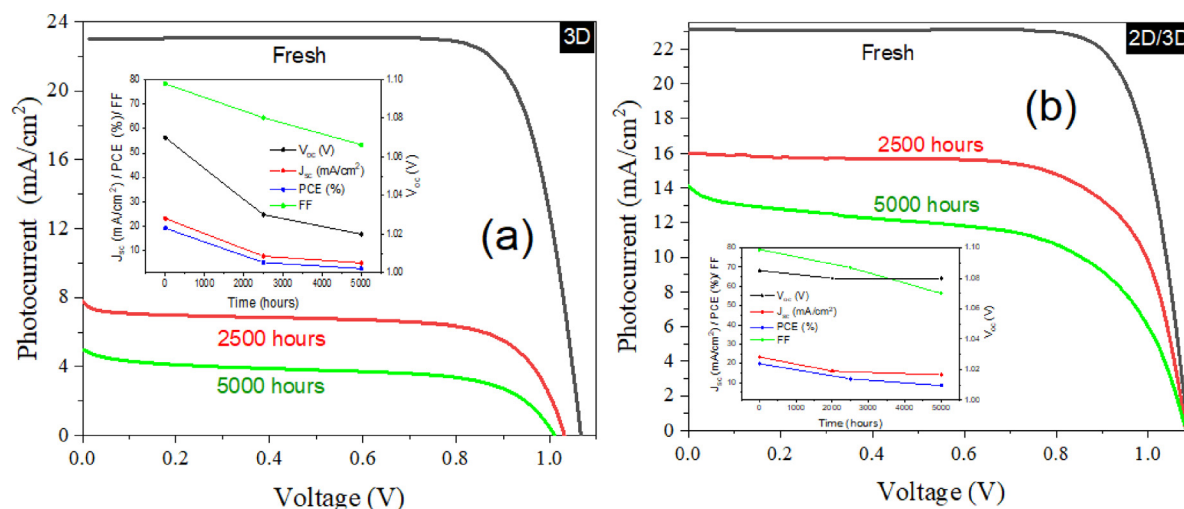


**Fig. 3.** Evolution of J-V characteristic curves with aging. (a) 3D PSC, (b) 2D/3D PSC. The measurements were taken for fresh samples, after 2500 h and after 5000 h. The insets show the behaviour of photovoltaic parameters over the period of 5000 h.

$\text{TiO}_2$ /perovskite and  $\text{m-TiO}_2$ /perovskite interfaces [23]. The EIS data obtained at all the potentials under illumination condition was fitted using the high potential current flow model (3 RC) in dark shown in Fig. 4, assuming that under illumination, the effect on EIS signal is

the same as providing a voltage source equal to  $V_{oc}$  (1.1 V, close to  $V_{oc}$  of the samples). In addition, a bisquert transmission line (BTO) model was also added to account for the light induced giant dielectric effect in the low-frequency [24,25].



**Table 1**

J-V parameters of 3D and 2D/3D samples including current density, open-circuit voltage, fill factor and power conversion efficiency.

Samples		$J_{sc}$ (mA/cm <sup>2</sup> )	$V_{oc}$ (V)	FF	Efficiency (%)
3D	Fresh	23.2	1.07	78.3	19.2
	2500 h	7.77	1.03	64.4	5.2
	5000 h	4.99	1.02	53.4	2.7
2D/3D	Fresh	23.3	1.085	79.2	19.8
	2500 h	16.0	1.08	69.7	12
	5000 h	14.1	1.08	56.4	8.6

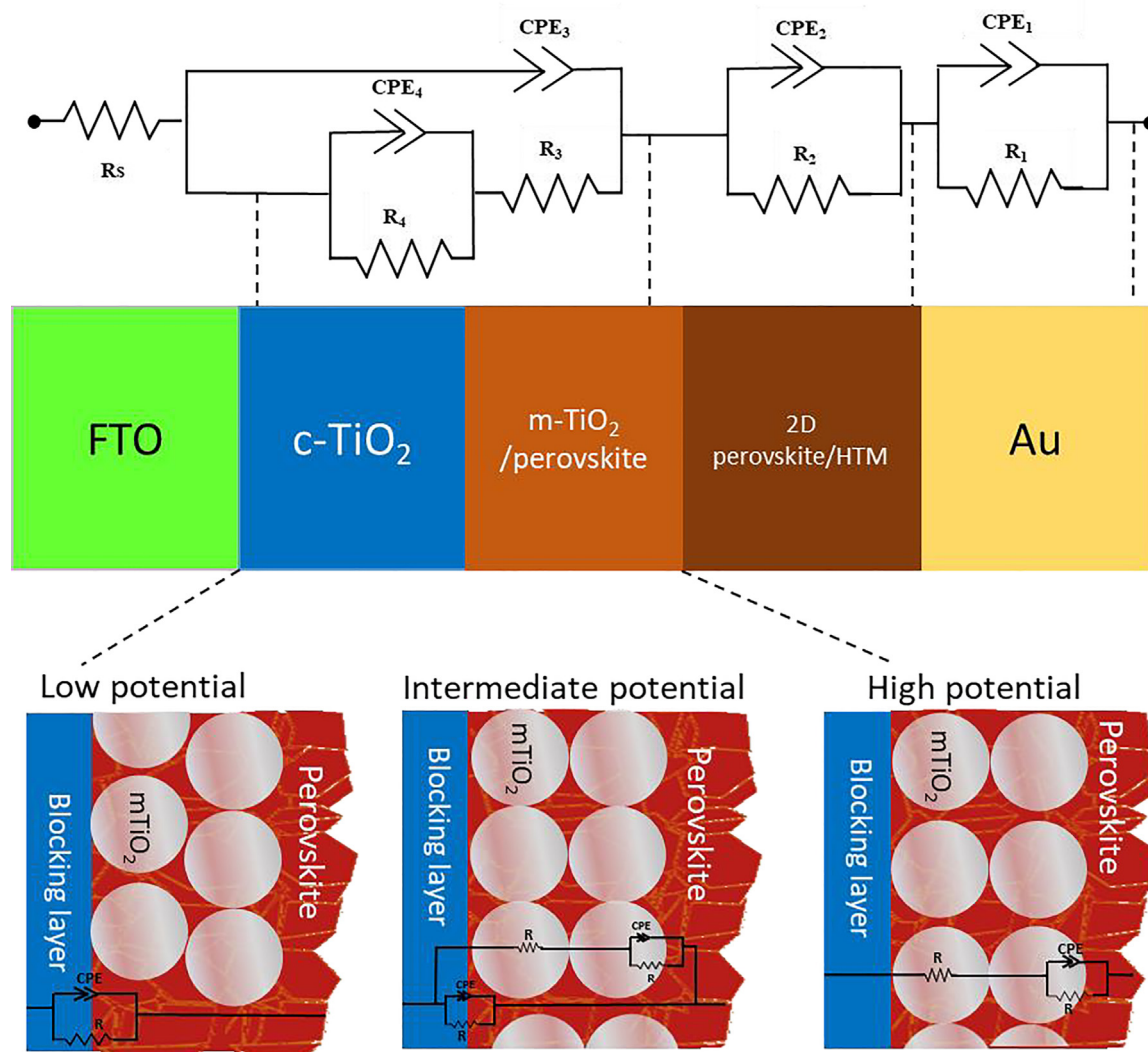


**Fig. 4.** Schematic explanation of electrical equivalent circuits (EEC) models used for impedance spectroscopy spectra fitting of 3D sample and 2D/3D samples. Each RC circuit assigned to their respected interfaces of the PSC architecture is also shown. The current follow model at low, intermediate and high potential in dark is also shown in the zoom in section. In light, the current follow model is assumed to behave similar to dark at high potential, for more detail please see the discussion section.

Fig. 5(a and b) shows the evolution of impedance spectra at 0 V in the dark with the passage of time while Fig. S1 (given in supplementary data file) exhibits the EIS plots at 0.5 V and 1.1 V. The extracted EIS parameters are presented in Table 3. One critical thing to notice in Fig. 5 is that the trend of the high frequency (HF) loop, which is attributed to  $R_{ct}$ , across Au/HTM/perovskite interface, is behaving oppositely in the 3D and 2D/3D sample. The  $R_{ct}$  decreases significantly with the passage of time in the case of 2D/3D sample (8.6 k $\Omega$   $\rightarrow$  3.3 k $\Omega$ ), whereas the  $R_{ct}$  of 3D sample is increasing with time (9.2 k $\Omega$   $\rightarrow$  15.1 k $\Omega$ ). Similar findings were made in previous work as well

[18]. This observation was backed up by bode plot analysis also, shown in Fig. 5(c and d). The admittance values ( $Y_{ct}$ ) corresponding to the HF loop, is also behaving in the opposite direction in both samples. Admittance of 2D/3D sample is increasing with the passage of time and vice versa. Admittance is a measure of current flow that is allowed by the device. Therefore, a higher admittance suggests a lower resistance to charge transfer. In addition, the peak frequencies ( $f_p$ ) representing the time constants associated with  $R_{ct}$  were also analyzed and it was clearly increasing in the case of 2D/3D sample (63.34 Hz  $\rightarrow$  198.6 Hz), while decreasing in the case of 3D sample

**Table 2**

EEC models developed for 3D and 2D/3D PSCs fitting at 0 V, 0.5 V and 1.1 V under dark and illumination conditions. This table was developed based on the current follow model shown in Fig. 4. At both low and high potentials (0 V and 1.1 V), 3 RC model has been proposed. Under 1 Sun illumination, at all applied potentials, same EEC model has been proposed as that of the high potential in dark, assuming the impedance response in light would reflect the response at an applied potential equal to  $V_{oc}$  in dark. Under light, the BTO element has been added in series with the low-frequency resistance component of the EEC model to represent photoinduced giant dielectric effect.

Applied potential	Illumination/ Dark conditions	EEC model
0 V, 1.1 V	Dark	
0.5 V	Dark	
0 V, 0.5 V, 1.1 V	1 Sun illumination	

(63.34 Hz  $\rightarrow$  24.93 Hz). The increase in  $f_p$  is represented by the shifting of the bode plot to the right indicating an increase in the conductivity at the high frequency region in 2D/3D sample. This increase in conductivity phase has been linked to Au penetration into the HTM layer in our previous work, which is backed up by EFISHG technique as well [18]. Nonetheless, both the solar cell types are showing degradation behavior with aging. The increase in  $R_{ct}$  value and a decrease in admittance and peak frequency, in the case of 3D sample indicates difficult charge extraction at the Au/HTM interface, while the decreasing  $R_{ct}$  trend and increasing admittance and peak frequency in the case of 2D/3D sample indicates the diminished role of HTM due to Au penetration [18], meaning that the charge transfer will now take place directly from Au to 2D perovskite. On the other hand, the decrease in  $f_p$  of 3D sample is exhibited by the shifting of the bode plot to the left which indicates a reduced conductivity phase of the 3D sample. Another crucial point to notice in Fig. 5(c and d) is that the 3D sample starts showing resistive behaviour after 5000 h, indicated by a horizontal line at  $0^\circ$  phase. While, in 2D/3D sample, this phenomenon was not observed with aging, suggesting better stability. Nonetheless, the  $f_p$  and  $R_{ct}$  value of both the samples were almost similar initially, indicating that the samples were not yet subjected to drastic degradation. Once the external environment starts affecting the samples, degradation begins and both the solar cell types degrade in separate manners at a different rate as discussed in [18]. It can also be observed in Fig. 5, that the intermediate-low frequency response which repre-

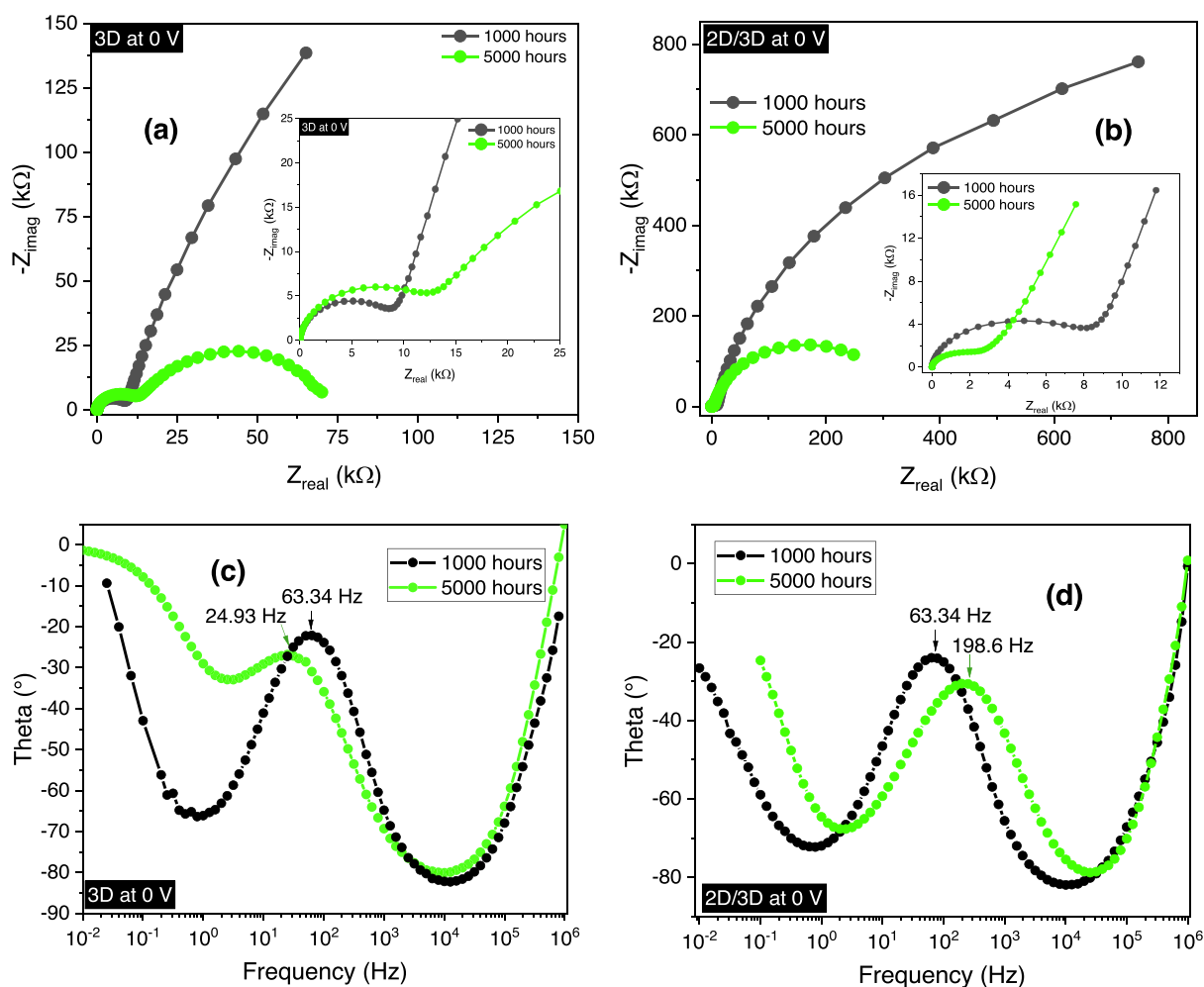


**Fig. 5.** Evolution of nyquist spectra in dark with aging at 0 V (a) 3D PSC and (b) 2D/3D. The insets in Fig. 5a & b show the zoom-in of the high-frequency semicircle. Fig. 5c & d show the bode plot evolution with aging at 0 V of 3D and 2D/3D samples, respectively. The measurements were taken after 1000 h and after 5000 h of aging.

**Table 3**

EIS parameters extracted from nyquist spectra and bode plot of 3D and 2D/3D samples after 1000 h and 5000 h. The nyquist spectra results are divided into high-frequency parameters and intermediate/low – frequency parameters showing the charge transfer and recombination resistance values. The bode plot results is showing the peak frequency values.

Sample	Aging time	Nyquist spectra results							Bode plot results
		HF region (Charge transfer)				IF/LF region (Recombination)			
		R <sub>s</sub> (Ω)	R <sub>ct</sub> (KΩ)	a <sub>ct</sub> (10 <sup>-3</sup> )	Y <sub>ct</sub> (10 <sup>-6</sup> )	R <sub>rec</sub> (KΩ)	a <sub>rec</sub> (10 <sup>-3</sup> )	Y <sub>rec</sub> (10 <sup>-6</sup> )	
3D	1000 h	12.84 ± 0.23	9.16	973.4	1.47	732.4	872	2.86	63.34
	5000 h	17.7 ± 0.31	15.1	969.9	0.176	76.5	800.6	3.44	24.93
2D/3D	1000 h	11.65 ± 0.21	8.6	968.8	0.067	1740	887.5	2.28	63.34
	5000 h	11.69 ± 0.23	3.35	994.4	0.582	336.9	871.8	2.49	198.6

sents the recombination resistance ( $R_{rec}$ ) either in the m-TiO<sub>2</sub> layer or in the bulk of the perovskite absorber, is decreasing significantly with time, and this is reflected in the decreasing PCEs of both 3D and 2D/3D samples. However, for 2D/3D sample, the  $R_{rec}$  value is still much higher than that of 3D sample for the same age and biasing conditions. Moreover,  $R_{rec}$  of 2D/3D sample decreases at a much slower rate as compared to that of the 3D sample. The  $R_{rec}$  of 3D sample decreases by approximately 90% (732.4 k $\Omega$   $\rightarrow$  76.5k $\Omega$ ) by the end of the aging cycle, while the  $R_{rec}$  of 2D/3D sample decreases by 79% (1740k $\Omega$   $\rightarrow$  336.9k $\Omega$ ).

### 3.1. Effect of voltage

The effect of different potentials on charge dynamics processes of both 3D and 2D/3D PSCs was also analysed by observing the  $R_{ct}$  and  $R_{rec}$  trend. Fig. 6 shows the nyquist plots obtained in dark at 0 V, 0.5 V and 1.1 V bias. It can be observed in Fig. 6 that the biasing voltage clearly influences the impedance spectra. The  $R_{ct}$  decreases with an increase in applied potential for both 3D and 2D/3D PSCs. This is because as the voltage is increased, electrons injection takes place from FTO into TiO<sub>2</sub> and perovskite, which induces an increase in the conductivity of the diode [26]. This can be understood by the Shockley equation;  $J = J_s(\exp \frac{V}{nV_T} - 1)$ . This relationship of current density with voltage decreases the resistance as the applied potential increases;  $R = (\frac{dJ}{dV})^{-1}$ . At 0 V, no current flows, however, when 0.5 V is applied, a minor current flow occurs in the forward direction, i.e., electrons are flowing from the FTO through the different layers and interfaces towards the gold contact. At 1.1 V, the flowing direct current becomes more important.

The EIS parameters extracted from the spectra are presented in Table 4. A close look at the parameters shows that the value of  $R_{ct}$  in the case of 2D/3D samples is slightly lower than that of 3D samples at all applied potentials. The  $R_{ct}$  of 3D sample decreases from 9.16  $\Omega$  to 6.55  $\Omega$  from 0 V to 1.1 V. While, the  $R_{ct}$  of 2D/3D sample decreases from 8.6  $\Omega$  to 3.43  $\Omega$ . The  $R_{ct}$  provided by the HTM/perovskite interface must be small in the case of 2D/3D samples because the 2D layer offers an extra step to the charge carriers. Moreover, typically, the deposition of HTM on the 2D layer is much smoother than that of the 3D layer (3D perovskite film usually has many voids between the grains of the 3D crystals). Hence, the poor perovskite/HTM/Au interface may be one of the potential reasons for the higher  $R_{ct}$  in 3D sample. Another critical point to notice is in the bode plots presented in Fig. 6 (c & d), at 1.1 V, where both the samples start showing strong resistive behaviours indicated by a decreased slope in the LF region of bode plots. A horizontal line represents a degraded device. It should also be noted that the HTM layer was doped with Lithium (Li), and Cobalt (Co) and the presence of Li<sup>+</sup> and Co<sup>2+</sup> enhanced its conductivity. When doping is performed, the Warburg element should also be considered. A Warburg impedance element can be challenging to recognize and is only observed at high doping levels. At HF, the Warburg impedance is small since holes and electrons do not have to move very far. At IF, the reactants must diffuse farther, thereby

increasing the Warburg impedance. Hence Warburg impedance is a value used to account mass charge transfer limitations due to diffusion processes adjacent to the electrode. However, in the current work, the Warburg element was not considered for EIS data fitting because the impurities did not appear to be high which was an assumption made from observing the EI spectra [4].

Next, analyzing the  $R_{rec}$ , it can be observed that the spectra at 0 V exhibits the largest semicircle in the IF – LF range followed by 0.5 V and 1.1 V for both 3D and 2D/3D PSC samples. This is because, the electron-hole density at 0 V across the perovskite interface is very low since there is no light source or external voltage provided to excite the electrons to the conduction band and it is limited by only the AC perturbation provided and the contribution from the back layer of the anode; c-TiO<sub>2</sub>/FTO. As the biasing voltage is increased, the electron-hole density increases as well and hence the recombination resistance decreases. At 1.1 V, higher forward current is passing through the different layers and interfaces, which significantly reduces the LF resistance;  $R_{rec}$  [27]. Nonetheless, it can be observed in Fig. 6, that the 2D/3D sample showed a higher value of  $R_{rec}$  compared to 3D sample for the same biasing conditions except for the applied bias 1.1 V.

Another approach to explain the effect of applied voltage on EI spectra can be represented by Fermi level splitting. When an external bias is applied to the PSC, the Fermi level of the device is forced to shift. As it can be observed in Fig. 7, once the biasing voltage is increased, the gap between the quasi-Fermi level of electrons and holes increases by downward shifting of  $E_{fp}$  (hole Fermi level), which reduces recombination losses. This is because the carrier density and Fermi level have an exponential relationship and recombination rate is directly affected by the current density [28]. In the case of 2D/3D sample, the additional 2D layer creates a larger Fermi level splitting hence further reducing the recombination losses [9]. This is because the additional 2D layer passivates the subgap defect states of the 3D layer (3D layer exhibits larger grains and hence many voids). Moreover, its downward shifted  $E_{fp}$  matches better with the HOMO level of HTM. All of these factors enhance the energy band alignment at the HTM/2D/3D perovskite interface and hence reduces recombination.

### 3.2. Effect of illumination

In addition, to study the charge dynamics processes under light, the EIS analysis was also performed under 1 sun illumination. The radiation of light is essential to the generation, movement and dissipation of some mobile ions [29,30]. Fig. 8 shows the evolution of impedance spectra of 3D and 2D/3D PSC devices at 0 V, 0.5 V and 1.1 V biasing under 1 sun illumination at different intervals of time. Table 5 presents the EI spectra results of 3D and 2D/3D sample. As the PSCs are kept under light, the electron-hole density across the perovskite increases, shifting its Fermi levels closer to the lower edge of the conduction band, thus resulting in a drastic change in all charge transfer resistances and interfacial capacitances. Before establishing a comparison between 3D and 2D/3D sample, it should be realized that the obtained

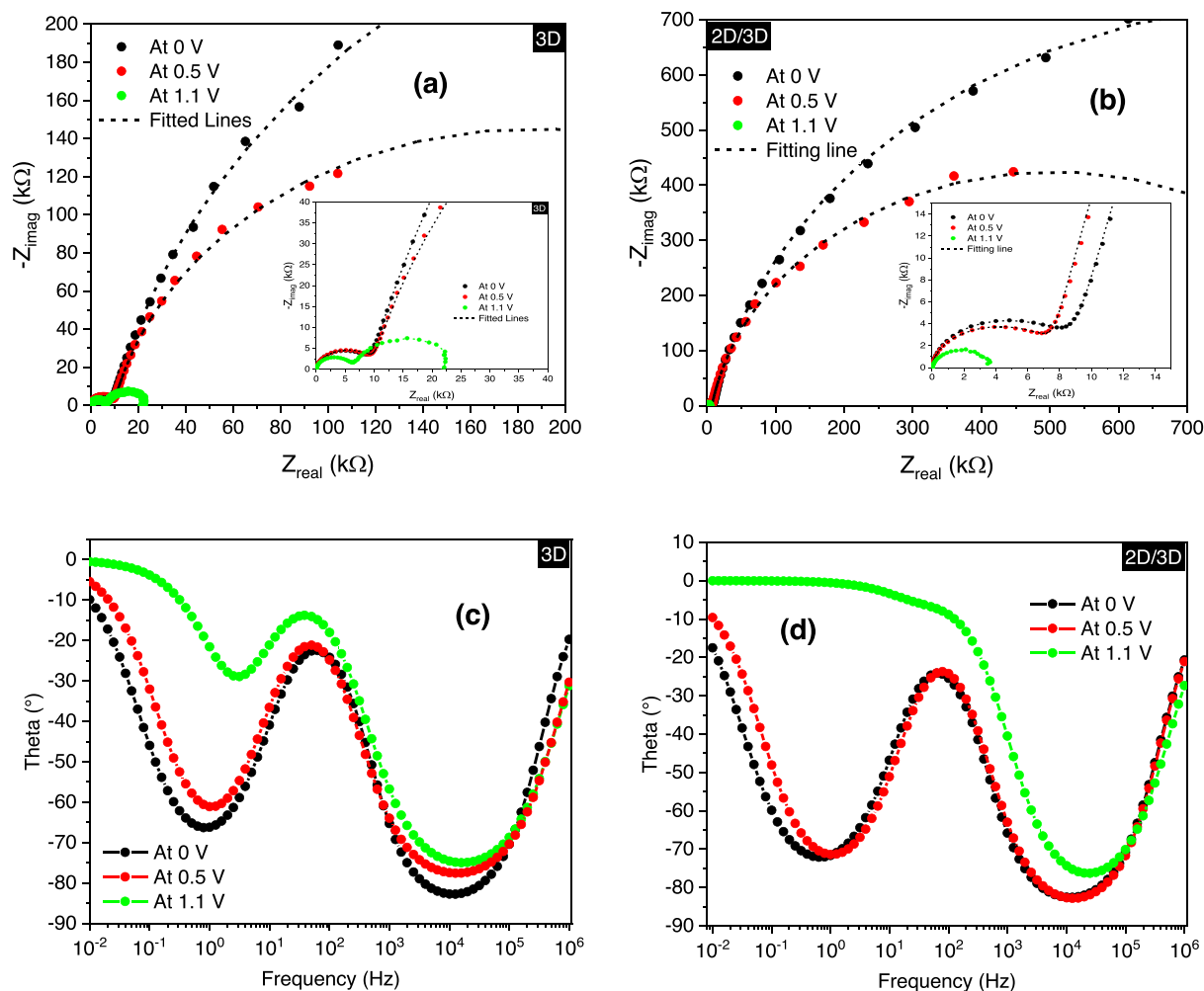


**Fig. 6.** Effect of the applied potential on the impedance spectra (IS) of the perovskite solar cells (PSCs). (a) 3D samples and (b) 2D/3D samples. These measurements are of 1000 h aged samples.

**Table 4**

Nyquist spectra results of 3D and 2D/3D samples obtained at 0 V, 0.5 V and 1.1 V in dark conditions at 10 mV perturbation.

Sample		Nyquist spectra results						
		HF region (Charge transfer)				IF/LF region (Recombination)		
		$R_s$ (Ω)	$R_{ct}$ (KΩ)	$\alpha_{ct}$ ( $10^{-3}$ )	$Y_{ct}$ ( $10^{-6}$ )	$R_{rec}$ (KΩ)	$\alpha_{rec}$ ( $10^{-3}$ )	$Y_{rec}$ ( $10^{-6}$ )
3D	0 V	$12.84 \pm 0.23$	9.16	973.4	0.059	732.4	872	2.86
	0.5 V	$10.5 \pm 0.31$	9.7	902.3	0.113	352.9	875.7	3.26
	1.1 V	$10.08 \pm 0.22$	6.55	880.7	0.148	16.6	884.8	8.74
2D/3D	0 V	$11.65 \pm 0.21$	8.6	968.8	0.067	1740	887.5	2.28
	0.5 V	$11.01 \pm 0.21$	7.13	979.9	0.079	1216	890	2.18
	1.1 V	$11.63 \pm 0.22$	3.43	921.5	0.086	1.01	911	8.65

EI spectra under illumination conditions were too complex to fit using the conventional EEC modeling method. Therefore, for simplification, an experimental fit was performed (as shown in Fig. S2) to extract the series resistance ( $R_s$ ) and the HF resistance;  $R_{ct}$ . The  $R_{rec}$  could not be extracted from Fig. 8 due to the significant distortion in the spectra. The simplified experimental fitting method shown in Fig. S2 (black dotted semicircles) was adopted for the EI spectra fitting under illumination conditions. When establishing a comparison between 3D and 2D/3D samples, one critical point to notice in Fig. 8 is that the trend of both  $R_{ct}$  and  $R_{rec}$  in the case of 2D/3D sample is totally opposite to that of 3D sample under illumination, at 0 V;  $R_{ct}$  of 2D/3D sample is decreasing with time ( $62.22 \Omega \rightarrow 31.9 \Omega$ ) while the  $R_{ct}$  of 3D sample

is increasing with time ( $48.31 \Omega \rightarrow 280.1 \Omega$ ). In the case of 3D sample, the 3D perovskite provides many voids for the HTM grains which can make it collapse against the 3D perovskite making the Au/HTM/perovskite contact irregular. Moreover, the 3D perovskite layer itself can collapse and undergo an irreversible decomposition into its precursor under ambient conditions [31]. Even though this phenomenon can be avoided by encapsulation, other illumination induced factors such as light soaking and ion migration can provoke degradation and can also give rise to anomalies such as J-V hysteresis. Therefore, charge extraction at this interface can become difficult increasing  $R_{ct}$  at Au/HTM/perovskite interface, with aging. On the other hand, in the case of 2D/3D sample, the dynamic behavior of 2D perovskite layer is



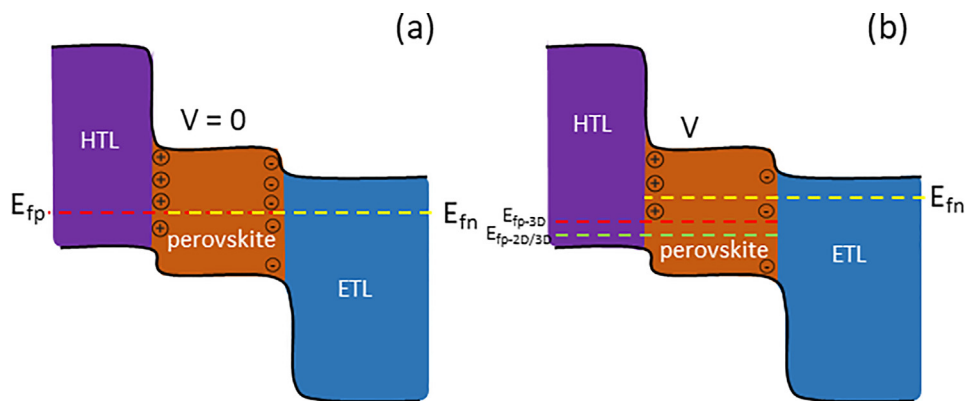


**Fig. 7.** Schematic illustration of energy level diagrams showing the Fermi level splitting at (a)  $V = 0$  V (no biasing) in dark condition and when biasing ( $V$ ) is applied (b).  $E_{fn}$  is the electron quasi-Fermi level and  $E_{fp}$  is the hole quasi-Fermi level. The figure was developed based on the understanding from [24] and [9].

assumed to be one of the major factors responsible for this trend in  $R_{ct}$ . 2D perovskite exhibits a much higher resistance to external environmental conditions compared to its 3D counterpart due to its larger cations, which hamper internal ionic motion and bring to the system the required organic moieties [7]. Moreover, the 2D layer on top of the 3D layer provides a smoother contact at the HTM/2D perovskite/3D perovskite interface which may prevent HTM from collapsing at HTM/perovskite interface. Subsequently, Au layer can penetrate into the HTM layer, with aging, which can be responsible for the decreasing  $R_{ct}$  trend [18] as discussed in dark EIS discussion. However, when potential is applied (0.5 V and 1.1 V), there is a difference in 3D sample's charge transfer behavior, and it now starts showing the same trend as the 2D/3D sample. This voltage induced behavior could be due to a disturbed flow of current. Nonetheless, when analyzing the data under illumination conditions with applied potential, it should be realized that the EI spectra are typically shifted to HF/IF region and the  $R_{rec}$  decreases significantly.

Apparently, the HF and LF time constants appear to be entirely merged after 5000 h at 0 V for the case of 3D sample. However, observing the spectra closely, it can be noticed that after 5000 h, the  $R_{rec}$  has decreased immensely indicating the degradation of the 3D sample. The  $R_{ct}$  is much bigger than the  $R_{rec}$  indicating that there is very little charge transfer because the electrons and holes are recombining before they can reach their respective electrodes. This effect could be due to resulting in degradation of 3D perovskite. In the case of 2D/3D sample, the 2D layer protects the 3D perovskite layer from harsh environmental conditions and hence it stays stable for long periods [9].

A negative capacitance feature has also been observed in the LF range for both 3D and 2D/3D samples under illumination. This feature can be attributed to the interfacial accumulation of charges across the perovskite/ $\text{TiO}_2$  interface [32]. One essential thing that can be noticed here is that this negative capacitance feature was observed in the dark only in the case of high biasing; 1.1 V, whereas in light, this feature has started to appear at low biasing. This is because the population of photoinduced electrons is higher in light as opposed to dark conditions and this can lead to interfacial charge accumulation. However, all this condition arises when m- $\text{TiO}_2$  which has been behaving as an insulator in the dark starts behaving as a semiconductor and charge transfer starts directly across perovskite and m- $\text{TiO}_2$  interface (as schematically explained in Fig. 4). Furthermore, a large amount of free charges is available, and they polarize across charge selective electrodes at low frequency. The current literature does not adequately describe all aspects of a LF loops of PSCs with experimental results, such as the systematic behaviour of the PSCs' physical processes under different conditions, the applicable EEC in the frequency and the time domain with the available EIS data [33]. The foremost necessary condition for the

negative capacitance is that the layer can be subjected to a great difference of Fermi levels at the Perovskite/HTM and Perovskite/m- $\text{TiO}_2$  layer but strong capacitive contacting structures. This condition is realized in the 3D and 2D/3D solar cells discussed in this work. Furthermore, these PSCs display a slightly irregular distribution of electrical fields in the complex morphological structure of the charge transport layer and introduced polarization.

After analyzing the impedance spectra in terms of resistances, a quantitative analysis with reference to changes in working frequency was also performed. The starting frequencies, peak frequencies and ending frequencies can be observed at the different time constants in Fig. 8. At 0 V, the HF peak of 3D sample is constant at 63.1 KHz in the first two cycles of measurements (1000 h and 2500 h). However, after 5000 h, the peak frequency seems to have decreased to 31 KHz. This is an indication of degradation of the perovskite/HTM/Au interface. The HF peak in 2D/3D sample does not seem to vary a lot and stays in the range of 50 to 60 KHz, at 0 V. At intermediate and high potentials; 0.5 V and 1.1 V, the HF peak is increasing with the passage of time in both the samples. One more thing that can be observed in Fig. 8 is that the HF peak in 2D/3D sample stays constant at 50.2 KHz at all applied potentials in the 3rd cycle. One explanation for this observation could be that there is a barrier that has formed which is limiting the charge transfer processes to a certain extent (or inhibiting charge transfer processes above a certain extent) and therefore there is no effect of increasing applied potential anymore. Another essential thing that can be observed in Fig. 8 is that the HF peaks of 3D and 2D/3D samples are similar at 0 V for the first two cycles. This means that the behavior of both the samples without an effect from applied voltage was similar until 2500 h and after the samples were aged for a long time, their behavior changed (after 5000 h).

#### 4. Conclusion

In this work, we adopted a phenomenological approach to study the effect of illumination and applied potential on the evolution of EI spectra of 3D and 2D/3D PSCs with aging. An advance EEC model was proposed which was modified based on applied potentials and illumination to ensure the validity and accuracy of the extracted fitting parameters, interpreting EI spectra. Through the analysis of resistance and peak frequency parameters, it was deduced that the Au/HTM/perovskite interface of 3D and 2D/3D sample behaves oppositely in terms of its charge transfer rate in the dark. The charge transfer resistance of 2D/3D sample decreases with time as opposed to that of the 3D sample. However, under illumination conditions, the 3D and 2D/3D samples show the same trend at intermediate and high potentials. Nonetheless, any increase or decrease in  $R_{ct}$  hinders the device's performance. Another information obtained from the EIS curves was that

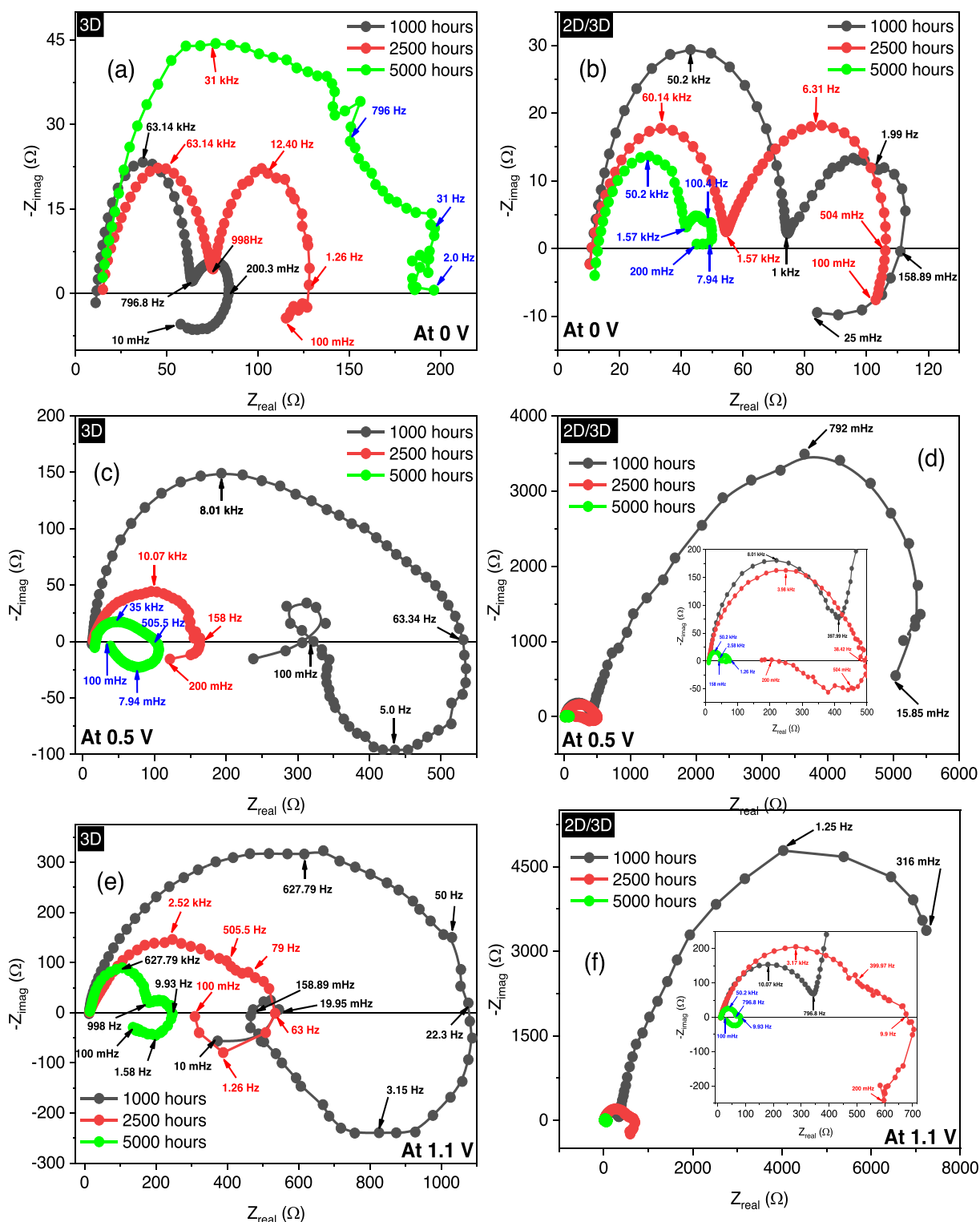


**Fig. 8.** Nyquist plots of the 3D (a) and 2D/3D (b) samples takes at different intervals of time (between the fabrication and 5000 h) under 1 sun illumination and at low DC applied potential. Figure (a & b) is obtained at 0 V. Figure (c & d) are obtained at 0.5 V. Figure (e & f) are obtained at 1.1 V.

a negative capacitance feature was observed under high biasing in the dark. While, under illumination conditions, the negative capacitance feature started to appear even at low potentials. Comparing the recombination resistance ( $R_{\text{rec}}$ ) at the perovskite/ $\text{TiO}_2$  interface of 3D and 2D/3D samples, it was observed the  $R_{\text{rec}}$  decreases in the case of both the solar cell types in the dark with aging and increasing potential, however, the rate of decrease was much smaller in 2D/3D sample

which revealed that adding the 2D capping layer enhances the stability of the device. These findings indicate that any change in applied potential or light conditions has a significant influence on the EI spectra. Moreover, the EI spectra at a fixed applied potential and illumination evolves with aging as well. We believe that further studies on EIS under varying conditions are necessary, especially under illumination since the EI spectra under light appeared to be complex to analyze and

**Table 5**

EI spectra parameters obtained at 0 V, 0.5 V and 1.1 V after 1000 h, 2500 h and 5000 h.

Sample	Aging time (hrs)	0 V		0.5 V		1.1 V	
		Rs ( $\Omega$ )	Rct ( $\Omega$ )	Rs ( $\Omega$ )	Rct ( $\Omega$ )	Rs ( $\Omega$ )	Rct ( $\Omega$ )
3D	1000	12.42 $\pm$ 0.26	48.31	13.99 $\pm$ 0.22	480	13.50 $\pm$ 0.23	1005
	2500	16.07 $\pm$ 0.51	50.98	14.1 $\pm$ 0.25	147.01	13.20 $\pm$ 0.26	500
	5000	16.5 $\pm$ 0.55	280.1	15.1 $\pm$ 0.25	95	13.21 $\pm$ 0.25	200.1
2D/3D	1000	11.80 $\pm$ 0.24	62.22	12.24 $\pm$ 0.34	536.5	11.58 $\pm$ 0.29	437.8
	2500	12.27 $\pm$ 0.21	40.9	11.42 $\pm$ 0.26	500	10.70 $\pm$ 0.26	499.5
	5000	13.5 $\pm$ 0.25	31.9	13.1 $\pm$ 0.33	21.1	11.08 $\pm$ 0.29	55.6

therefore further experiments are vital to validate and elucidate the findings.

### CRediT authorship contribution statement

**Sumayya M. Abdulrahim:** Methodology, Data curation, Writing – original draft. **Zubair Ahmad:** Conceptualization, Methodology, Supervision, Validation, Writing – review & editing. **Muhammad Qasim Mehmood:** Writing – review & editing. **Sanghyun Paek:** Methodology. **J. Bhadra:** Writing – review & editing. **Noora J. Al-Thani:** Writing – review & editing. **Mohammad Khaja Nazeeruddin:** Writing – review & editing. **Abdelhak Belaidi:** Writing – review & editing. **Mahmood Amani:** Writing – review & editing.

### Declaration of Competing Interest

The authors declare that they have no known competing financial interests or personal relationships that could have appeared to influence the work reported in this paper.

### Funding

This publication was made possible by NPRP award [NPRP11S-1210-170080] from Qatar National Research Fund (a member of Qatar Foundation). The findings made herein are solely the responsibility of the authors.

### Appendix A. Supplementary data

Supplementary data to this article can be found online at <https://doi.org/10.1016/j.jelechem.2021.115800>.

### References

- [1] M.A. Green, E.D. Dunlop, J. Hohl-Ebinger, M. Yoshita, N. Kopidakis, A.W.Y. Ho-Baillie, Solar cell efficiency tables (Version 55), *Progress in Photovoltaics: Research and Applications* 28 (1) (2019) 3–15.
- [2] J.Y. Kim, J.-W. Lee, H.S. Jung, H. Shin, N.-G. Park, High-Efficiency Perovskite Solar Cells, *Chem Rev* 120 (15) (2020) 7867–7918.
- [3] M.S. Abbas, S. Hussain, J. Zhang, B. Wang, C. Yang, Z. Wang, Z. Wei, R. Ahmad, Orientationally engineered 2D/3D perovskite for high efficiency solar cells, *Sustainable Energy & Fuels* 4 (1) (2020) 324–330.
- [4] Z. Ahmad, T. Noma, S. Paek, K.T. Cho, D. Taguchi, M. Iwamoto, T. Manaka, M.K. Nazeeruddin, F. Touati, S.A. Al-Muhtaseb, Stability in 3D and 2D/3D hybrid perovskite solar cells studied by EFISHG and IS techniques under light and heat soaking, *Organic Electronics* 66 (2019) 7–12.
- [5] H.S. Choi, H.S. Kim, 3D/2D Bilayered Perovskite Solar Cells with an Enhanced Stability and Performance, *Materials (Basel)* 13 (17) (2020) 3868.
- [6] G. Grancini, C. Roldan-Carmona, I. Zimmermann, E. Mosconi, X. Lee, D. Martineau, S. Narbey, F. Oswald, F. De Angelis, M. Graetzel, M.K. Nazeeruddin, One-Year stable perovskite solar cells by 2D/3D interface engineering, *Nat Commun* 8 (2017) 15684.
- [7] A. Krishna, S. Gotti, M.K. Nazeeruddin, F. Sauvage, Mixed Dimensional 2D/3D Hybrid Perovskite Absorbers: The Future of Perovskite Solar Cells?, *Advanced Functional Materials* 29 (8) (2019) 1806482, <https://doi.org/10.1002/adfm.201806482>.
- [8] K.T. Cho, G. Grancini, Y. Lee, E. Oveisi, J. Ryu, O. Almora, M. Tschumi, P.A. Schouwink, G. Seo, S. Heo, J. Park, J. Jang, S. Paek, G. Garcia-Belmonte, M.K. Nazeeruddin, Selective growth of layered perovskites for stable and efficient photovoltaics, *Energy & Environmental Science* 11 (4) (2018) 952–959.
- [9] P. Chen, Y. Bai, S. Wang, M. Lyu, J.-H. Yun, L. Wang, In Situ Growth of 2D Perovskite Capping Layer for Stable and Efficient Perovskite Solar Cells, *Advanced Functional Materials* 28 (17) (2018) 1706923, <https://doi.org/10.1002/adfm.201706923>.
- [10] P. Jiang, Y. Xiong, M.I. Xu, A. Mei, Y. Sheng, L.I. Hong, T.W. Jones, G.J. Wilson, S. Xiong, D. Li, Y. Hu, Y. Rong, H. Han, The Influence of the Work Function of Hybrid Carbon Electrodes on Printable Mesoscopic Perovskite Solar Cells, *The Journal of Physical Chemistry C* 122 (29) (2018) 16481–16487.
- [11] Z. Wang, Q. Lin, F.P. Chmiel, N. Sakai, L.M. Herz, H.J. Snaith, Efficient ambient-air-stable solar cells with 2D–3D heterostructured butylammonium-caesium-formamidinium lead halide perovskites, *Nature Energy* 2 (9) (2017) 17135.
- [12] X. Chen, Y. Shirai, M. Yanagida, K. Miyano, Effect of Light and Voltage on Electrochemical Impedance Spectroscopy of Perovskite Solar Cells: An Empirical Approach Based on Modified Randles Circuit, *The Journal of Physical Chemistry C* 123 (7) (2019) 3968–3978.
- [13] L. Contreras-Bernal, S. Ramos-Terrón, A. Riquelme, P.P. Boix, J. Idígoras, I. Mora-Seró, J.A. Anta, Impedance analysis of perovskite solar cells: a case study, *Journal of Materials Chemistry A* 7 (19) (2019) 12191–12200.
- [14] J. Xing, Q.I. Wang, Q. Dong, Y. Yuan, Y. Fang, J. Huang, Ultrafast ion migration in hybrid perovskite polycrystalline thin films under light and suppression in single crystals, *Phys Chem Chem Phys* 18 (44) (2016) 30484–30490.
- [15] B.J. Kolber, J.M. Janjic, J.A. Pollock, K.J.J.B.m.e. Tidgewell, Summer undergraduate research: A new pipeline for pain clinical practice and research 16 (2016) 1–11.
- [16] A. Mahapatra, N. Parikh, P. Kumar, M. Kumar, D. Prochowicz, A. Kalam, M.M. Tavakoli, P. Yadav, Changes in the Electrical Characteristics of Perovskite Solar Cells with Aging Time, *Molecules* 25 (10) (2020) 2299.
- [17] Dino Klotz, Ganbaatar Tumen-Ulzii, Chuanjiang Qin, Toshinori Matsushima, Chihaya Adachi, Detecting and identifying reversible changes in perovskite solar cells by electrochemical impedance spectroscopy, *RSC Advances* 9 (57) (2019) 33436–33445.
- [18] Z. Ahmad, A. Mishra, S.M. Abdulrahim, D. Taguchi, P. Sanghyun, Consequence of Aging at Au/HTM/perovskite interface in triple cation 3D and 2D/3D hybrid perovskite solar cells, *Scientific Reports Article is in press* (2021).
- [19] Z. Ahmad, F. Aziz, H.Y. Abdullah, Study on the stability of the mixed (MAPbI3 and MAPbBr3) perovskite solar cells using dopant-free HTL, *Organic Electronics* 76 (2020) 105453.
- [20] S.M. Abdulrahim, Z. Ahmad, J. Bhadra, N.J. Al-Thani, Long-Term Stability Analysis of 3D and 2D/3D Hybrid Perovskite Solar Cells Using Electrochemical Impedance Spectroscopy, *Molecules* 25 (24) (2020) 5794.
- [21] D. Wei, G. Amaratunga, Photoelectrochemical cell and its applications in optoelectronics, *Int. J. Electrochem. Sci.* 2 (2007) 897–912.
- [22] Kun Cao, Zhixiang Zuo, Jin Cui, Yan Shen, Thomas Moehl, Shaik M. Zakeeruddin, Michael Grätzel, Mingkui Wang, Efficient screen printed perovskite solar cells based on mesoscopic TiO2/Al2O3/NiO/carbon architecture, *Nano Energy* 17 (2015) 171–179.
- [23] Z. Ahmad, A. Mishra, S.M. Abdulrahim, F. Touati, Electrical equivalent circuit (EEC) based impedance spectroscopy analysis of HTM free perovskite solar cells, *Journal of Electroanalytical Chemistry* (2020).
- [24] D. Moia, I. Gelmetti, P. Calado, W. Fisher, M. Stringer, O. Game, Y. Hu, P. Docampo, D. Lidzey, E. Palomares, J. Nelson, P.R.F. Barnes, Ionic-to-electronic current amplification in hybrid perovskite solar cells: ionically gated transistor-interface circuit model explains hysteresis and impedance of mixed conducting devices, *Energy & Environmental Science* 12 (4) (2019) 1296–1308.
- [25] Emilio J. Juarez-Perez, Rafael S. Sanchez, Laura Badia, Germá Garcia-Belmonte, Yong Soo Kang, Ivan Mora-Sero, Juan Bisquert, Photoinduced Giant Dielectric Constant in Lead Halide Perovskite Solar Cells, *J Phys Chem Lett* 5 (13) (2014) 2390–2394.
- [26] F. Ebadi, N. Taghavinia, R. Mohammadpour, A. Hagfeldt, W. Tress, Origin of apparent light-enhanced and negative capacitance in perovskite solar cells, *Nat Commun* 10 (1) (2019) 1574.
- [27] Isaac Zarazua, Guifang Han, Pablo P. Boix, Subodh Mhaisalkar, Francisco Fabregat-Santiago, Ivan Mora-Seró, Juan Bisquert, Germá Garcia-Belmonte, Surface Recombination and Collection Efficiency in Perovskite Solar Cells from Impedance Analysis, *J Phys Chem Lett* 7 (24) (2016) 5105–5113.
- [28] D. Pitarch-Tena, T.T. Ngo, M. Vallés-Pelarda, T. Pauporté, I. Mora-Seró, Impedance Spectroscopy Measurements in Perovskite Solar Cells: Device Stability and Noise Reduction, *ACS Energy Letters* 3 (4) (2018) 1044–1048.
- [29] Silvia Colella, Michela Todaro, Sofia Masi, Andrea Listorti, Davide Altamura, Rocco Caliendo, Cinzia Giannini, Elisa Carignani, Marco Geppi, Daniele

- Meggiolaro, Gianpiero Buscarino, Filippo De Angelis, Aurora Rizzo, Light-Induced Formation of  $Pb^{3+}$  Paramagnetic Species in Lead Halide Perovskites, *ACS Energy Letters* 3 (8) (2018) 1840–1847.
- [30] H.S. Kim, I. Mora-Sero, V. Gonzalez-Pedro, F. Fabregat-Santiago, E.J. Juarez-Perez, N.G. Park, J. Bisquert, Mechanism of carrier accumulation in perovskite thin-absorber solar cells, *Nat Commun* 4 (2013) 2242.
- [31] Giulia Grancini, Mohammad Khaja Nazeeruddin, Dimensional tailoring of hybrid perovskites for photovoltaics, *Nature Reviews Materials* 4 (1) (2019) 4–22.
- [32] Francisco Fabregat-Santiago, Michael Kulbak, Arava Zohar, Marta Vallés-Pelarda, Gary Hodes, David Cahen, Iván Mora-Seró, Deleterious Effect of Negative Capacitance on the Performance of Halide Perovskite Solar Cells, *ACS Energy Letters* 2 (9) (2017) 2007–2013.
- [33] Dino Klotz, Negative capacitance or inductive loop? – A general assessment of a common low frequency impedance feature, *Electrochemistry Communications* 98 (2019) 58–62.